ELSEVIER

IUMRS-ICA 2011

Alloy Design for High-Entropy Bulk Glassy Alloys

A. Takeuchi[a],*, N. Chen[a], T. Wada[b], W. Zhang[b],
Y. Yokoyama[b], A. Inoue[a] and J.-W. Yeh[c]

[a] *World Premier International Research Center (WPI), Tohoku University, Sendai 980-8577, Japan*
[b] *Institute for Materials Research, Tohoku University, Sendai 980-8577, Japan*
[c] *Department of Materials Science and Engineering, National Tsing Hua University, Hsinchu 300, Taiwan, ROC.*

Abstract

An efficient alloy design for bulk metallic glasses (BMGs) assisted by a composition–configurational entropy (C-CE) diagram has been proposed by introducing a feature of high-entropy (HE) alloys that are defined by an equi-atomic alloy with five or more elements. The proposed alloy design compensated for a shortcoming in determining the compositions of BMGs and led to success in forming a $Pd_{20}Pt_{20}Cu_{20}Ni_{20}P_{20}$ HE-BMG with a maximum diameter of 10 mm. The C-CE diagram demonstrates the equi-atomicity of alloys, providing candidates for HE-BMGs. The alloy design for HE-BMG will promise opening up the new cutting-edge in both HE alloys and BMGs.

Keywords: Bulk metallic glass; high-entropy alloy; alloy design

1. Introduction

Recently, bulk metallic glasses (BMGs) [1,2] and high-entropy (HE) alloys [3,4] have been accumulating unprecedented academic and engineering interest in a field of advanced metallic materials. The recent increasing interest for BMGs and HE alloys is due to their unique structures and resultant superior properties than those of conventional crystalline alloys. Here, BMGs are defined as a subset of metallic glasses formed with a critical diameter (d_c) of a couple of millimeters or more. The superior properties of BMGs as well as metallic glasses against conventional crystalline alloys are principally due to features of metallic glasses, such as the glass transition in temperature and resultant supercooled liquid

*A. Takeuchi. Tel.: +81-22-217-5956; Fax: +81-22-217-5956.
E-mail address: takeuchi@wpi-aimr.tohoku.ac.jp

range, and a non-crystalline amorphous/glassy structure. On the other hand, HE alloys are defined as multicomponent alloys comprising five or more elements with perfect as well as partially-imperfect equiatomic composition where the former and the latter were categorized as HE alloys of narrow and wide senses, respectively, by Takeuchi et al [4]. The HE alloys also exhibits superior properties than conventional crystalline alloy owing to their unique structures, which prevent the complicated intermetallic compounds from forming. Specifically, HE alloys are principally composed of a simple crystalline structure of fcc or bcc or their mixture as well as a rarely formed amorphous structure in a shape of thin film [3, 4] for systems with metalloid elements. An example of the superior properties of HE alloys includes increase in mechanical properties than the conventional crystalline alloys [3, 4]. Thus, the BMGs with amorphous structure and HE alloys comprising principally crystalline structures are thought to be different advance metallic materials. However, recent reports on $Pd_{20}Pt_{20}Cu_{20}Ni_{20}P_{20}$ [5] and $Zn_{20}Ca_{20}Sr_{20}Yb_{20}(Li_{0.55}Mg_{0.45})_{20}$ [6] alloys revealed that new BMGs with a characteristic of HE alloys have begun to be found as HE-BMGs in multicomponent systems.

Very recently, the authors have reported [5] that a $Pd_{20}Pt_{20}Cu_{20}Ni_{20}P_{20}$ HE alloy can be produced as a BMG with a critical diameter of 10 mm by referring to a ternary prototype of $Pd_{40}Ni_{40}P_{20}$ BMG [7]. This HE-BMG is the first success in merging HE alloys of narrow sense and BMGs. In addition, this alloy is the first success in HE-BMGs in Metal-Metalloid type, which includes metalloid elements from B, C, Si, P and Ge. The success in fabricating HE-BMG is considerably important when considering the mutual progress in the development of both BMGs and HE alloys. However, there remain a plenty of unknown features of HE-BMGs, since the history of HE-BMGs has just started. For instance, unknown features of HE-BMGs include that the $Pd_{20}Pt_{20}Cu_{20}Ni_{20}P_{20}$ HE-BMG has not yet optimized for the components as HE-BMGs of narrow sense and that HE-BMGs of narrow sense in Metal–Metal type comprising metallic elements solely have yet been discovered to date. To make matters worth, one cannot avoid searching for new BMGs in multicomponent systems with elements more than four because of the saturating number of BMGs found to date up to quaternary alloys. Hence, it is important to consider efficient alloy design for BMGs to shorten consuming time and to reduce manual labor for the development of new BMGs.

The present study aims to develop Metal–Metalloid type of HE-BMG of narrow sense, to analyze the compositional features of these HE-BMGs and to assess the efficiency of the alloy design for HE-BMG.

2. Methods

2.1. Sample preparation and analysis

We studied $Pd_{20}Pt_{20}(TM1)_{20}(TM2)_{20}P_{20}$ alloys in nominal atomic percentages where TM1 and TM2 are transition metals from Fe, Co, Ni and Cu. Specifically, we studied (TM1,TM2) = (Co,Cu), (Co,Fe), (Fe,Cu) and (Cu,Ni), but we did not deal with (TM1,TM2) = (Fe,Ni), (Co,Ni). The latter results will be reported somewhere else in near future. The specimens with diameters of 3 and 5 mm were prepared by conventional copper mold casting method after master alloys from pure substances had been prepared in advance by arc melting in an argon atmosphere. When a BMG is formed with copper mold casting, then, water quenching with B_2O_3 flux treatment was tried to form a BMG with greater dimensions in a capsuled quartz tube. Structural analysis of the samples was conducted using X-ray diffraction (XRD).

2.2. A Composition–Configurational Entropy (C-CE) Diagram

An especial composition diagram was created to analyze the relationships between the compositions (C) and configurational entropy ($S_{config.}$:CE) for HE-BMGs, HE alloys, BMGs and conventional alloys. Examples of the C-CE diagrams for ternary and quaternary alloys are shown in Figs. 1 and 2, respectively.

The composition diagram has plots in three-dimensional space (x,y,z), where the base (x,y,0) corresponds to a composition diagram comprising a regular polyhedron depending on the number of constituent elements (N). On the other hand, the vertical axis (z) expresses $S_{config.}/S_{config.(ideal)}$ value where the $S_{config.}/S_{config.(ideal)} = \ln N$ [3, 5]. In the C-CE diagram, the coordinates of vertices on the base to form a polyhedron, which corresponds to those of pure constituent elements, are expressed by Eqs. (1) and (2).

$$x_i = \cos (2\pi i/N) \qquad (i = 0, 1, 2, …, N\text{-}1) \qquad (1)$$

$$y_i = \sin (2\pi i/N) \qquad (i = 0, 1, 2, …, N\text{-}1) \qquad (2)$$

Thus, the coordinates of the plot of an alloy (x,y) were calculated by summing up the components expressed by Eqs. (1) and (2) separately after multiplying the fraction of the i-th element (c_i). Specifically, x and y are expressed by Eqs. (3) and (4),

$$x = \Sigma\, c_i\, x_i \qquad\qquad\qquad\qquad (3)$$

$$y = \Sigma\, c_i\, y_i \qquad\qquad\qquad\qquad (4)$$

On the other hand, the value of z can be calculated by Eq. (5),

$$z = S_{config.}(x,y)/ S_{config.(ideal)}(0,0) = (- \Sigma\, c_i \ln c_i)/ \ln N \qquad (5)$$
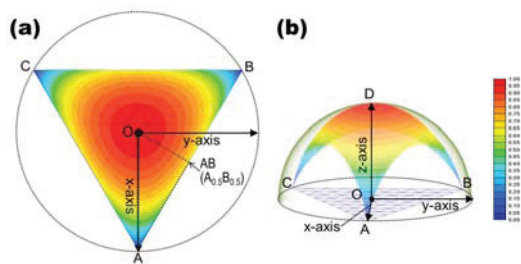

Fig. 1 Composition–configurational entropy (C-CE) diagram for an A-B-C ternary system: (a) A conventional triangle (Gibbs) composition diagram with contour lines for z values given by Eq. (5). There vertices (A, B, C) have a distance of unity from the origin (O). The area surrounded by the triangle A-O-AB is the intrinsic composition in an $A_aB_bC_c$ alloy that satisfies a ≥ b ≥ c; (b) Three-dimensional C-CE diagram where the distance DO is unity, forming a hemisphere with a radius of unity.
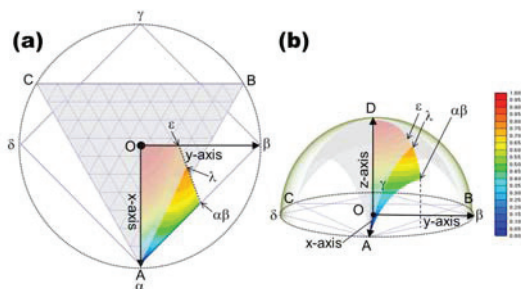

Fig. 2 Composition–configurational entropy (C-CE) diagram for a α-β-χ-δ quaternary system where the C-CE diagram is drawn to inscribe a sphere with a radius of unity. The hatches in gray demonstrate the data for an A-B-C ternary system shown in Fig. 1 for comparison. (a) A square composition diagram in which the intrinsic compositions of the $α_aβ_bχ_cδ_d$ alloy that satisfies a ≥ b ≥ c ≥ d are drawn in a quadrangle O-α-αβ-ε. (b) Three-dimensional C-CE diagram. Alloys with a composition in an area O-α-λ-ε have smaller z-value than that for an A-B-C ternary system.

In the C-CE diagram, all the HE alloy with perfect equi-atomicity are plotted at $(x,y,z) = (0,0,1)$, whereas the pure elements are plotted on the base at a vertex at a radius of unity from the origin. We determined to arrange the constituent elements on the base as follows. The constituent element with the greatest fraction in composition was set up at the vertex of $(1,0,0)$. Then, the vertices located at the next in anticlockwise direction were occupied in the order of decreasing fraction of the composition. This arrangement of the constituent elements made the plots of alloys on the base at the first quadrant principally. The distance between the plots traced on x-y plane and the origin exhibit the degree of equi-atomicity of an alloy. Thus, the distance from the origin and the z-value identify the feature of alloys in C-CE diagram.

3. Results and Discussion

3.1. HE-BMG

Figure 3 shows an outer surface and cross-sectional images and XRD diffraction pattern from the cross-sectional area of the $Pd_{20}Pt_{20}Ni_{20}Cu_{20}P_{20}$ alloy prepared by water-quenching with B_2O_3 flux treatment [5]. As shown in Fig. 3(a), the cylindrical samples exhibit good metallic luster, indicating the sample surfaces are neither oxidized and nor contaminated due to the effect of B_2O_3 on excluding impurities other than the constituent elements. Furthermore, observations of the sample surfaces with unaided eyes can explain the absence of a concave shape on the millimeters to sub-millimeter scales. The XRD pattern in Fig. 3(b) taken from the cross-sectional area in Fig. 3(a) demonstrates the formation of a glassy single phase in $Pd_{20}Pt_{20}Cu_{20}Ni_{20}P_{20}$ alloy with a diameter of 10 mm [5].

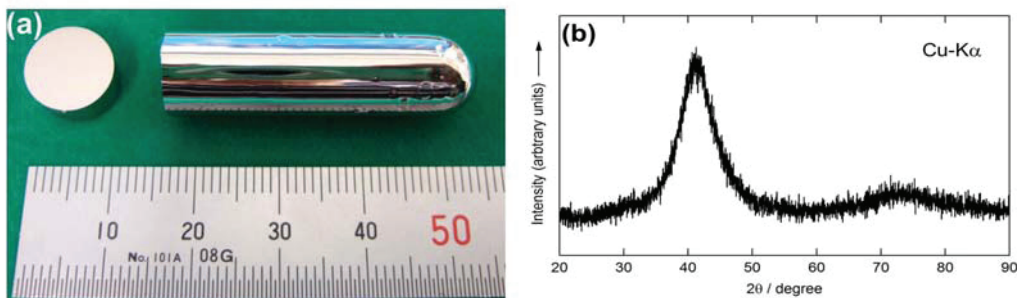Fig. 3 (a) Outer surface and cross-sectional images and (b) XRD pattern from a cross-sectional area of a $Pd_{20}Pt_{20}Cu_{20}Ni_{20}P_{20}$ cylinder with 10 mm in diameter prepared by water quenching with B_2O_3 fluxed treatment [5].

On the other hand, the XRD patterns shown in Fig. 4 revealed that $Pd_{20}Pt_{20}(TM1)_{20}(TM2)_{20}P_{20}$ alloys including TM1 and TM2 other than Cu and Ni shown as XRD profiles (a)–(f) are formed in a mixture structure from fcc, bcc and monoclinic phases for specimens even in smaller diameters ranging 3–5 mm. Thus, it was found that $(TM1,TM2) = (Cu,Ni)$ shown as XRD profile (g) is the only possible combinations for the alloy series to be formed in HE-BMG. The reason for the formation of BMGs including an atomic pair of Cu-Ni is explained by the meat of mixing (ΔH_{mix}) [8, 9] summarized in Table 1 and the information of phase diagrams [10]. The Cu-Ni atomic pair has a positive value of $\Delta H_{mix} = +4$ kJmol^{-1}, whereas Cu-Co and Cu-Fe atomic pairs have a greater positive ΔH_{mix} values of $+ 6$ kJmol^{-1} and $+13$ kJmol^{-1}, respectively. Besides, on the phase diagrams Cu-Ni exhibits solid solutions over an entire composition, whereas Cu-Co and Cu-Fe exhibit immiscible composition region. Besides the alloys studied in the present study, $(TM1,TM2) = (Fe,Ni)$ and (Co,Ni) are expected as the candidates of HE-

BMGs because of their values of ΔH_{mix} are –2 and 0 kJmol^{-1}, respectively. In addition, both (TM1,TM2) = (Fe,Ni) and (Co,Ni) exhibit entire formation of solid solutions on the phase diagram. These considerations explain that the formation of HE-BMG for (TM1,TM2) = (Cu,Ni) is due to avoidance of the phase separation tendencies of the atomic pair. Further researches for the alloys (TM1,TM2) = (Fe,Ni), (Co,Ni) will be reported the results somewhere else in near future.
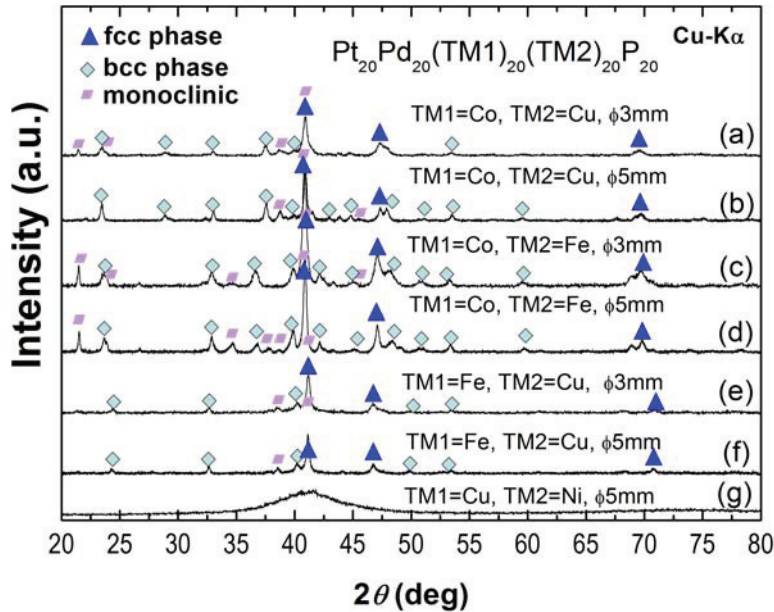

Fig. 4 XRD patters of $Pd_{20}Pt_{20}(TM1)_{20}(TM2)_{20}P_{20}$ cylinders with 3 and 5 mm in diameter prepared by copper mold casting. (TM1,TM2) = (Co,Cu), (Co,Fe), (Fe,Cu) and (Cu,Ni).

Table 1. Mixing enthalpy (ΔH_{mix}) in the units of kJmol^{-1} at binary equi-atomic compositions for atomic pairs [8, 9] for $Pd_{20}Pt_{20}(TM1)_{20}(TM2)_{20}P_{20}$ alloy where (TM1,TM2) = (Co,Cu), (Co,Fe), (Fe,Cu) and (Cu,Ni). Asterisk indicates the atomic pairs, which were not studied in the present study.

ΔH_{mix}	Pd	Pt	Ni	Cu	P	Fe
Pd	—	+2	0	−14	−36.5	−4
Pt	+2	—	−5	−12	−34.5	−13
Ni	0	−5	—	+4	−34.5	−2*
Cu	−14	−12	+4	—	−17.5	+13
P	−36.5	−34.5	−34.5	−17.5	—	−39.5

3.2. C-CE Diagram for HE-BMGs

Figure 5 shows the C-CE diagram for HE-BMGs and BMGs. Figure 5 contains plots of $Pd_{20}Pt_{20}Cu_{20}Ni_{20}P_{20}$ [5] with alloy No. 25 and $Zn_{20}Ca_{20}Sr_{20}Yb_{20}(Li_{0.55}Mg_{0.45})_{20}$ [6] with alloy No. 26 as HE-BMGs of a narrow and wide senses, respectively. The other plots in Fig. 5 are BMGs with d_c of half-inch (~ 1.27 cm) or more with Nos. 1–18 [11–26] analyzed in our previous work [27], and other BMGs with Nos. 19–23 [28–31]. The C-CE diagram clearly indicates that $Pd_{20}Pt_{20}Ni_{20}Cu_{20}P_{20}$ alloy is plotted at

(0,0,1), indicating that the $Pd_{20}Pt_{20}Ni_{20}Cu_{20}P_{20}$ alloy is the HE-BMG of a narrow sense. On the other hand, the $Zn_{20}Ca_{20}Sr_{20}Yb_{20}(Li_{0.55}Mg_{0.45})_{20}$ alloy with a high z-value of 0.98 ~ 1 is plotted near the origin in the x-y plane, indicating that the $Zn_{20}Ca_{20}Sr_{20}Yb_{20}(Li_{0.55}Mg_{0.45})_{20}$ alloy is a HE-BMG of the wide sense. Besides, the BMGs in the centimeter with d_c of half-inch (~ 1.27 cm) with Nos. 1– 18 [11–26] are plotted ranging $0.66 < z < 0.98$. Among the alloys listed in Table 2, Pd- and Pt-based BMGs, such as Nos. 1, 3 and 8 tend to have high z value, whereas Zr- and La-based BMGs with Nos. 7, 11, 18, 21 and 22 has lower z-values. The Be-containing Zr-based BMG (Vit1) with No. 2 has a high z-value of 0.9, but this alloy is not plotted near the origin in x-z plane as the Pd- and Pt-based BMGs. This feature of Vit1 suggests that Vit1 cannot be a candidate of HE-BMG. On the other hand, it is noted that $Y_{36}Sc_{20}Al_{24}Co_{20}$ BMG with No. 9 has a high z-value of 0.98 and its position at x-y plane is as close to that of the $Zn_{20}Ca_{20}Sr_{20}Yb_{20}(Li_{0.55}Mg_{0.45})_{20}$ HE-BMG of a wide sense. This feature of $Y_{36}Sc_{20}Al_{24}Co_{20}$ BMG indicates that Metal-Metal type HE-BMG of a narrow sense will be found by modifying a composition slightly from $Y_{36}Sc_{20}Al_{24}Co_{20}$ BMG. We will report the results of Metal-Metal type HE-BMG of a narrow sense somewhere else in in near future. Thus, Fig. 5 indicates that a reason for the $Pd_{20}Pt_{20}Cu_{20}Ni_{20}P_{20}$ formable as a HE-BMG is due to its prototype of $Pd_{40}Ni_{40}P_{20}$ BMG, which is located at a nearest the origin among the BMGs listed in Table 2. Thus, the C-CE diagram indicates the candidates of the future HE-BMGs by its positions in the diagram.
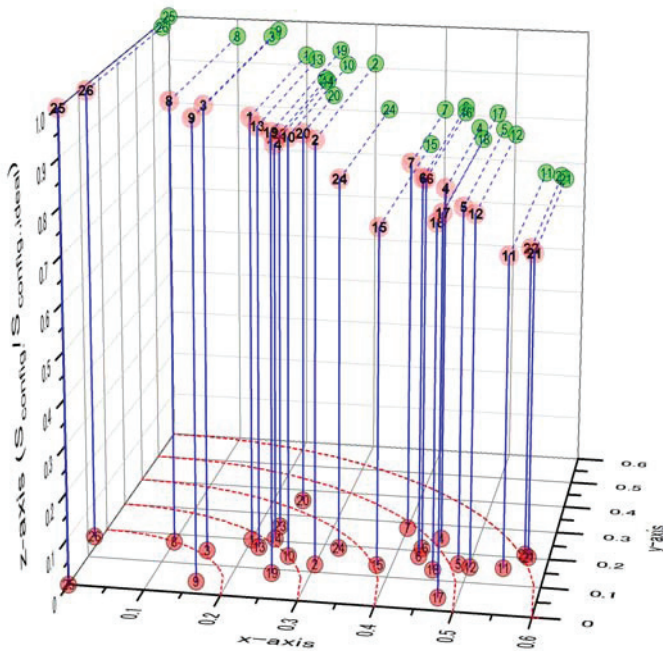

Fig. 5 Composition–configurational entropy (C-CE) diagram for HE-BMGs and BMGs. The plots (pink) with alloy numbers in Table 2 exhibit the (x,y,z) calculated by Eqs. (3)–(5). The dots (light green) on the x-z plane, which are drawn by tracing the plots, are to show the z-value comprehensively. The $Pd_{20}Pt_{20}Cu_{20}Ni_{20}P_{20}$ HE-BMG (Alloy No. 25) has a plot at (0,0,1). The distance of the plots traced on the base (x-y plane) form the origin (0,0,0) indicates the degree of equi-atomicity of alloys.

Table 2 Bulk metallic glasses, their critical diameters (d_c) and their references. Alloys with Nos. 1–18 are BMGs with d_c of half-inch (~ 1.27 cm) or more, which were analyzed in the authors' previous study [27]. Alloys with Nos. 19–23 are newly added as d_c ≥ half-inch in the present study and those with Nos. 25 and 26 are HE-BMGs. Alloy with No. 24 is the prototype of Alloy No. 14.

No	Alloy	d_c / mm	z	Ref.
1	$Pd_{40}Cu_{30}Ni_{10}P_{20}$	72	0.92	[11]
2	$Zr_{41.2}Ti_{13.8}Cu_{12.5}Ni_{10}Be_{22.5}$ (Vit1)	>50	0.91	[12]
3	$Pd_{35}Pt_{15}Cu_{30}P_{20}$	30	0.96	[13]
4	$Zr_{55}Al_{10}Ni_5Cu_{30}$	30	0.77	[14]
5	$Mg_{59.5}Cu_{22.9}Ag_{6.6}Gd_{11}$	27	0.77	[15]
6	$Mg_{54}Cu_{26.5}Ag_{8.5}Gd_{11}$	25	0.82	[16]
7	$Zr_{48}Cu_{36}Ag_8Al_8$	25	0.81	[17]
8	$Pd_{40}Ni_{40}P_{20}$	25	0.96	[18]
9	$Y_{36}Sc_{20}Al_{24}Co_{20}$	25	0.98	[19]
10	$(La_{0.7}Ce_{0.3})_{65}Co_{25}Al_{10}$	25	0.90	[20]
11	$La_{62}(Cu_{5/6}Ag_{1/6})_{14}Ni_5Co_5Al_{14}$	>20	0.68	[21]
12	$Zr_{57}Ti_5Cu_{20}Ni_8Al_{10}$	20	0.76	[22]
13	$Pt_{42.5}Cu_{27}Ni_{9.5}P_{21}$	20	0.92	[23]
14	$(Fe_{0.8}Co_{0.2})_{48}Cr_{15}Mo_{14}C_{15}B_6Tm_2$	16	0.87	[24]
15	$Pt_{60}Cu_{16}Ni_2P_{22}$	16	0.73	[23]
16	$Mg_{54}Cu_{28}Ag_7Y_{11}$	16	0.81	[16]
17	$Ca_{65}Mg_{15}Zn_{20}$	>15	0.81	[25]
18	$Zr_{58.5}Nb_{2.8}Cu_{15.6}Ni_{12.8}Al_{10.3}$	15	0.75	[26]
19	$Ni_{50}Pd_{30}P_{20}$	21	0.94	[28]
20	$Pd_{40}Ni_{40}Si_4P_{16}$	20	0.83	[29]
21	$Zr_{61}Ti_2Nb_2Al_{7.5}Ni_{10}Cu_{17.5}$	20	0.66	[30]
22	$Zr_{60}Ti_2Nb_2Al_{7.5}Ni_{10}Cu_{18:5}$	20	0.67	[30]
23	$Ti_{40}Zr_{25}Cu_{12}Ni_3Be_{20}$	14	0.87	[31]
24	$Fe_{48}Cr_{15}Mo_{14}Er_2C_{15}B_6$	12	0.81	[32]
25	$Pd_{20}Pt_{20}Cu_{20}Ni_{20}P_{20}$	10	1	[5]
26	$Zn_{20}Ca_{20}Sr_{20}Yb_{20}(Li_{0.55}Mg_{0.45})_{20}$	>3	0.98	[6]

4. Conclusions

The $Pd_{20}Pt_{20}(TM1)_{20}(TM2)_{20}P_{20}$ alloys where (TM1,TM2) = (Co,Cu), (Co,Fe), (Fe,Cu) and (Cu,Ni) in Metal–Metalloid type were experimentally studied in the present work. The results revealed that $Pd_{20}Pt_{20}Cu_{20}Ni_{20}P_{20}$ is formed in HE-BMG with a critical diameter of 10 mm, but other alloys with atomic pairs excepting for (TM1,TM2) = (Cu,Ni) were not formed in BMGs. The composition–configurational entropy (C-CE) diagrams proposed in the present study efficiently express the degree of equi-atomicity,

leading to suggesting candidates of HE-BMGs from BMGs found to date. The alloy design with a concept of HE alloys accompanied by C-CE diagram is useful for the further development of HE-BMGs.

Acknowledgements

References

[1] Inoue A, Takeuchi A. Recent Development and Application Products of Bulk Glassy Alloys. *Acta Mater* 2011; **59:2243**–2267.

[2] Inoue A. Stabilization of Metallic Supercooled Liquid and Bulk Amorphous Alloys. *Acta Mater* 2000; **48:279**–306.

[3] Yeh J-W, Chen S-K, Lin S-J, Gan J-Y, Chin T-S, Shun T-T, Tsau C-H, Chang S-Y. Nanostructured High-Entropy Alloys with Multiple Principal Elements: Novel Alloy Design Concepts and Outcomes. *Adv Eng Mater* 2004; **6:299**–303.

[4] Yeh J-Y. Recent progress in High-Entropy Alloys. *Ann Chim Sci Mat* 2006; **31:633**–648.

[5] Takeuchi A, Chen N, Wada T, Yokoyama Y, Kato H, Inoue A, Yeh J-W. $Pd_{20}Pt_{20}Cu_{20}Ni_{20}P_{20}$ High-Entropy Alloy as a Bulk Metallic Glass in the Centimeter. *Intermetallics* 2011; **19:1546**–1554.

[6] Zhao K., Xia X.X., Bai H.Y., Zhao D.Q., Wang W.H. Room Temperature Homogeneous Flow in a Bulk Metallic Glass with Low Glass Transition Temperature. *Appl Phys Lett* 2011; **98**:141913.

[7] Drehman A.J., Greer A.L. Kinetics of Crystal nucleation and Growth in $Pd_{40}Ni_{40}P_{20}$ Glass. *Acta Metall* 1984; **32:323**–332.

[8] In: de Boer FR, Pettifor DG, series editors. *Cohesion in Metals Transition Metal Alloys*, Elsevier Science Publishers B.V., Amsterdam, 1988.

[9] Takeuchi A, Inoue A. Classification of Bulk Metallic Glasses by Atomic Size Difference, Heat of Mixing and Period of Constituent Elements and Its Application to Characterization of the Main Alloying Element. *Mater Trans* 2005; **46:2817**–2829.

[10] Okamoto H. *Desk Handbook Phase Diagrams for Binary Alloys*, Second Edition, ASM International, Materials Park, Ohio, 2010.

[11] Inoue A, Nishiyama N, Kimura HM. Preparation and Thermal Stability of Bulk Amorphous $Pd_{40}Cu_{30}Ni_{10}P_{20}$ Alloy Cylinder of 72 mm in Diameter. *Mater Trans, JIM* 1997; **38:179**–183.

[12] Johnson W.L. Fundamental Aspects of Bulk Metallic Glass Formation in Multicomponent Alloys. *Mater Sci Forum* 1996; **225–227**:35–50.

[13] Nishiyama N, Takenaka K, Wada T, Kimura HM, Inoue A. Undercooling Behavior and Critical Cooling Rate of Pd-Pt-Cu-P Alloy. *Mater. Trans* 2005; **46:2807**–2810.

[14] Inoue A, Zhang T. Fabrication of Bulk Glassy $Zr_{55}Al_{10}Ni_5Cu_{30}$ Alloy of 30 mm in Diameter by a Suction Casting Method. *Mater Trans, JIM* 1996; **37:185**–187.

[15] Zheng Q, Xu J, Ma E. High Glass-Forming Ability Correlated with Fragility of Mg-Cu(Ag)-Gd Alloys. *J Appl Phys* 2007; **102:113519**.

[16] Ma H, Shi L L, Xu J, Li Y, Ma E. Discovering Inch-Diameter Metallic Glasses in Three-Dimensional Composition Space. *Appl Phys Lett* 2005; **87:181915**.

[17] Zhang W, Zhang QS, Qin CL, Inoue A. Synthesis and Properties of Cu-Zr-Ag-Al Glassy Alloys with High Glass-Forming Ability. *Mater Sci Eng* 2008; **B148:92**–96.

[18] He Y, Schwarz RB., Archuleta JI. Bulk Glass Formation in the Pd-Ni-P System . *Appl Phys Lett* 1996; **69:1861**–1863.

[19] Guo FQ, Poon SJ, Shiflet GJ. Metallic Glass Ingots Based on Yttrium. *Appl Phys Lett* 2003; **83**:2575–2577.

[20] Li R, Pang S, Ma C, Zhang T. Influence of Similar Atom Substitution on Glass Formation in (La-Ce)-Al-Co Bulk Metallic Glasses. *Acta Mater* 2007; **55**:3719-3726.

[21] Jiang QK, Zhang GQ, Chen LY, Wu JZ, Zhang HG, Jiang JZ. Glass Formability, Thermal Stability and Mechanical Properties of La-Based Bulk Metallic Glasses. *J Alloys Comp* 2006; **424:183**–186.

[22] Xing L.Q., Ochin P. Bulk Glass Formation in the Zr-Ti-Al-Cu-Ni System. *J Mater Sci Lett* 1997; **16**; 1277–1280.

[23] Schroers J, Johnson WL. Highly Processable Bulk Metallic Glass-Forming Alloys in the Pt-Co-Ni-Cu-P System. *Appl Phys Lett* 2004; **84:3666**–3668.

[24] Amiya K, Inoue A. Fe-(Cr, Mo)-(C, B)-Tm Bulk Metallic Glasses with High Strength and High Glass-Forming Ability. *Rev Adv Mater Sci* 2008; **18:27**–29.

[25] Park ES, Kim DH. Formation of Ca-Mg-Zn Bulk Glassy Alloy by Casting into Cone-Shaped Copper Mold. *J Mater Res* 2004; **19:685**–688.

[26] Busch R, Mauhr A, Bakke E, Johnson WL. Bulk Metallic Glass Formation from Strong Liquids. *Mater Sci Forum* 1998; **269–272**:547–552.

[27] Takeuchi A, Yavari AR, Inoue A. Golden Mean Analysis of Bulk Metallic Glasses with Critical Diameter over Half-Inch for their Mole Fractions of Compositions. *Intermetallics* 2009; **17:696**–703.

[28] Zeng YQ, Nishiyama N, Yamamoto T, Inoue A. Ni-Rich Bulk Metallic Glasses with High Glass-Forming Ability and Good Metallic Properties. *Mater Trans* 2009; **50:2441**–2445.

[29] Chen N, Yang HA, Caron A, Chen PC, Lin YC, Louzguine-Luzgin DV, Yao KF, Esashi M., Inoue A. Glass-Forming Ability and Thermoplastic Formability of a $Pd_{40}Ni_{40}Si_4P_{16}$ glassy alloy. *J Mater Sci* 2011; **46:2091**–2096.

[30] Inoue A, Zhang QS, Zhang W, Yubuta K, Son KS, Wang XM. Formation, Thermal Stability and Mechanical Properties of Bulk Glassy Alloys with a Diameter of 20 mm in Zr-(Ti,Nb)-Al-Ni-Cu System. *Mater Trans* 2009; **50:388**–394.

[31] Guo FQ, Wang HJ, Poon SJ, Shiflet GJ. Ductile Titanium-Based Glassy Alloy Ingots. *Appl Phys Lett* 2005; **86:091907**.

[32] Ponnambalam V, Poon SJ, Shiflet GJ. Fe-Based Bulk Metallic Glasses with Diameter Thickness Larger than One Centimeter. *J Mater Res* 2004;**19**:1320–1323.